A Design Algorithm for Multivariable Linear Quadratic Integral Controllers in Voltage-Source Converters

Andres F. Lopez-Chavarro
Electrical and Computer Eng. Dept.
University of Puerto Rico
Mayaguez, Puerto Rico
andres.lopez23@upr.edu

Juan F. Patarroyo-Montenegro
Electrical and Computer Eng. Dept.
University of Puerto Rico
Mayaguez, Puerto Rico
juan.patarroyo@upr.edu

Enrique A. Sanabria-Torres
Electrical and Computer Eng. Dept.
University of Puerto Rico
Mayaguez, Puerto Rico
enrique.sanabria@upr.edu

Daniel D. Campo-Ossa
Electrical and Computer Eng. Dept.
University of Puerto Rico
Mayaguez, Puerto Rico
daniel.campo@upr.edu

Jesus D. Vasquez-Plaza
Electrical and Computer Eng. Dept.
University of Puerto Rico
Mayaguez, Puerto Rico
jesus.vasquez@upr.edu

Fabio Andrade-Rengifo
Electrical and Computer Eng. Dept.
University of Puerto Rico
Mayaguez, Puerto Rico
ORCID: 0000-0002-8859-7336

***Abstract*—This paper presents a voltage control design algorithm for a three-phase voltage source converter (VSC) connected to a linear load using a passive LCL filter. The controller is based on an optimal regulator, combined with the integral of the voltage error, which is called LQI that achieves null tracking of the error. The main objective of this paper is to present an algorithm to design a voltage controller through frequency analysis of the singular values of the system, the weight of the states involved in the system, the movement of the closed poles and their respective step response to evaluate performance and robustness against load changes. The simulation results show a satisfactory operation of the voltage controller with fast recovery after a resistive load change.**

Keywords—Multivariable Control, Three-Voltage Source Converter, Linear Quadratic Integral Controller, Singular Values, Optimal Control, Microgrid controllers.

I. BACKGROUND

Microgrid control is typically separated into different hierarchical levels [1]: V-I Control, primary control, secondary control, and tertiary control. V-I control level regulates the inverter's output signal waveform in order to meet power quality requirements such as amplitude, frequency, and harmonic distortion. Primary control regulates power-sharing between generators and the main grid. Secondary control regulates microgrid power quality. Finally, tertiary control manages issues related to energy markets such as microgrid power-sharing to the main grid, controlling battery usage, predicting energy production values, demand response against sudden generator changes, etc. From these control levels, V-I control level is the baseline for developing the other control levels.

The V-I control level regulates inverter's output voltage and current. A typical V-I control scheme for an inverter generator is shown in fig. 1. The control objectives of the V-I control level include perfect tracking of the voltage or current reference signal, harmonic rejection caused by nonlinear loads, and robustness against load changes. To achieve these objectives, many different control strategies have been proposed in literature [2]. Classical controllers refer to Laplace-domain controllers with typical structures such as P, PI, or PID controllers. These controllers are commonly used due to their "tuning" nature that makes their implementation quite straightforward. Some of the applications of PI controllers for the V-I control level are presented in [3]–[7]. One of the main drawbacks of these works is that the control gains are found heuristically without considering the model of the inverter.

Optimal and are based on improving inverter performance according a defined objective function. Optimal controllers such as the Linear-Quadratic Regulator (LQR) are aimed to minimize the energy in the states and inputs. The most common implementation of LQR controllers for inverter control is the well-known Linear-Quadratic Integrator (LQI). This control method has the advantage of being robust by nature providing infinite gain margin and a minimum phase margin of 60 degrees [8]. Some of the relevant works related to optimal control using LQI controllers may be found in [9]–[13]. Most of these approaches show the mathematical formulation of the LQI controller. However, there are no works in the literature focused on showing how to select the weighting matrices Q and R.

One of the most common approaches to select the values of Q and R is presented in [8]. The author suggests to start selecting the diagonal elements of Q and R as the inverse of the maximum quadratic value of the corresponding state-variable or input. Although this method presents a good start point, the selection of the final Q and R is a process that requires knowledge of the dynamics of the plant and the control objectives.

In this work, an algorithm for designing an LQI controller for voltage-source inverters is presented. This design algorithm analyzes the closed-loop eigenvalues, the singular value diagram, and the simulated step-response to define suitable values of Q and R. Although this algorithm demonstrates adequate results, the final definition of the weighting matrices will always depend on the designer expertise on the control application.

The rest of this document is organized as follows: section II shows the model used for the design of the LQI controller. Section III presents the design algorithm for the LQI controller. Finally, simulation results are presented in section IV.

II. SYSTEM MODELING

The system structure shown in fig. 1 is composed of three blocks organized in decrease order. The first one is the VSC connected to load through LCL filter considering the series resistance R_i in each inductor L_i. The second one is transformation blocks from abc to dq-axes from an angular frequency of 377 rad/sec corresponding to operation angular frequency ω_c. The final block is the voltage controller. The new variables connected to discretization block ZOH arrives at the optimal control system block which contains the feedback gain K_{LQI} y two additional stated variables corresponding to a delay time in the control signal and the integral of the voltage error in the capacitor. The Model neglects the PWM switching frequency.

A. Continuos-time mathematical model

Before designing any controller, it is necessary to know the mathematical model of the system to analyze stability and check control requirements, for instance, the controllability of the system. This requirement allows us to infer the existence of a feedback gains matrix that takes the trajectory of the system states from a starting point to a final point in a finite time [14]. Using the first-order differential equations through Kirchhoff currents and voltage analysis, the mathematical model for the system shown in fig.1 is obtained and transformed in to the dq frame [15]. The state-space model is given by

$$\begin{aligned}\dot{\vec{x}}(t) &= \boldsymbol{A}\vec{x}(t) + \boldsymbol{B}\vec{u}(t)\\ \vec{y}(t) &= \boldsymbol{C}\vec{x}(t)\end{aligned} \tag{1}$$

where the state vector is

$$\vec{x}(t) = \begin{bmatrix} I_{1d} & I_{1q} & I_{2d} & I_{2q} & Vc_d & Vc_q \end{bmatrix}^T(t) \tag{2}$$

and matrices $\boldsymbol{A}$, $\boldsymbol{B}$, $\boldsymbol{C}$ are expressed as (3).

B. Discrete-time mathematical model

The discretization of the system in the state space is done using the Zero Order Hold method (ZOH) with a sampling time T_s. Thus, the system is given by

$$\begin{aligned}\vec{x}\{k+1\} &= \boldsymbol{G}\vec{x}\{k\} + \boldsymbol{H}\vec{u}\{k\}\\ \vec{y}\{k\} &= \boldsymbol{C}\vec{x}\{k\}\end{aligned} \tag{4}$$

where matrices $\boldsymbol{G}$ and $\boldsymbol{H}$ are obtained as

$$\boldsymbol{G} = e^{\boldsymbol{A}\cdot T_s} \qquad \boldsymbol{H} = \left(\int_0^{T_s} e^{\boldsymbol{A}\cdot\tau}\, d\tau\right)\cdot \boldsymbol{B} \tag{5}$$

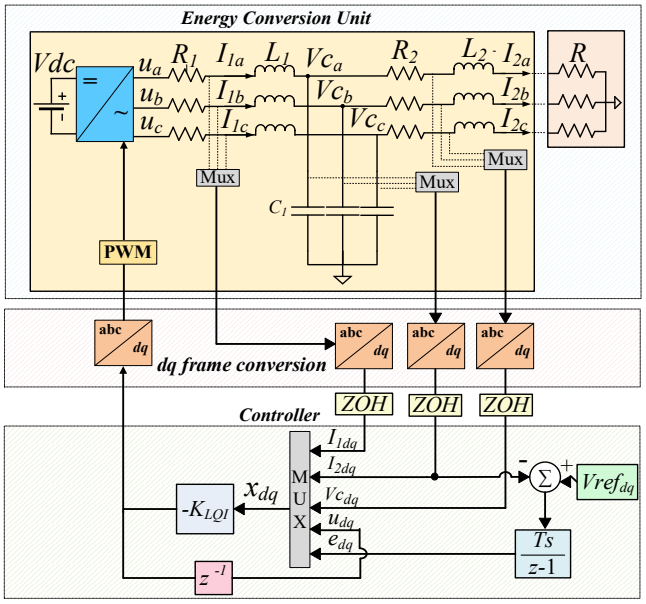

Fig. 1. Control Structure for VSC.

During the computational time, a delay appears at the input to the system. Therefore, it is necessary to take it into account in the system, and the matrices $\boldsymbol{G}$, $\boldsymbol{H}$, and $\boldsymbol{C}$ are augmented with a new state as follows

$$\begin{aligned}\boldsymbol{G_d} &= \begin{bmatrix}\boldsymbol{G} & \boldsymbol{H}\\ \emptyset & \emptyset\end{bmatrix}\\ \boldsymbol{H_d} &= [\emptyset \quad \boldsymbol{I}]^T\\ \boldsymbol{C_d} &= [\boldsymbol{C} \quad \emptyset]\end{aligned} \tag{6}$$

where the subscript 'd' denotes the matrices increased with computational delay and '$\emptyset$' denotes matrix of zeros with convenient size. Thus, the new state vector is

$$\overrightarrow{x_d}\{k+1\} = [\,\vec{x} \quad | \quad d_{in}]^T\{k+1\} \tag{7}$$

and the system in state space becomes

$$\begin{aligned}\overrightarrow{x_d}\{k+1\} &= \boldsymbol{G_d}\overrightarrow{x_d}\{k\} + \boldsymbol{H_d}\vec{u}\{k\}\\ \vec{y}\{k\} &= \boldsymbol{C_d}\overrightarrow{x_d}\{k\}\end{aligned} \tag{8}$$

C. Linear Quadratic Controller

Optimal quadratic control provides several advantages over other control techniques since it obtains a matrix of state feedback gains that brings the poles of the closed-loop system to the location where the best performance of the transient response is obtained, in addition to providing robustness

$$\boldsymbol{A} = \begin{bmatrix} -R_1/L_1 & \omega_c & 0 & 0 & -1/L_1 & 0\\ -\omega_c & -R_1/L_1 & 0 & 0 & 0 & -1/L_1\\ 0 & 0 & -(R_2+R)/L_2 & \omega_c & 1/L_2 & 0\\ 0 & 0 & -\omega_c & -(R_2+R)/L_2 & 0 & 1/L_2\\ 1/C_1 & 0 & -1/C_1 & 0 & 0 & \omega_c\\ 0 & 1/C_1 & 0 & -1/C_1 & -\omega_c & 0 \end{bmatrix} \tag{3}$$

$$\boldsymbol{B} = \begin{bmatrix} 1/L_1 & 0 & 0 & 0 & 1 & 0\\ 0 & 1/L_1 & 0 & 0 & 0 & 1 \end{bmatrix}^T \qquad \boldsymbol{C} = \begin{bmatrix} 0 & 0 & 0 & 0 & 1 & 0\\ 0 & 0 & 0 & 0 & 0 & 1 \end{bmatrix}$$

against to deviations. The main control objective is to minimize the cost function

$$J = \frac{1}{2}\sum_{k=0}^{N-1}(x_k^* \boldsymbol{Q} x_k + u_k^* \boldsymbol{R} u_k) \quad (9)$$

where $\boldsymbol{Q}$ and $\boldsymbol{R}$ are positive semidefinite and positive definite hermetic matrices, respectively, where their values on the diagonal are assigned based on the importance of the states of the system under study.

Therefore, the control problem is reduced to determine the control law $u = -\boldsymbol{K}x(t)$, where $\boldsymbol{K}$, for multivariate systems, is a matrix of constant gains found by solving the Ricatti Algebraic Equation (ARE) of (10) [16]. This control law obtains the desired trajectories of the system with optimal performance [8].

$$\boldsymbol{G^T S + SG - SHR^{-1}H^T S + C^T QC = 0} \quad (10)$$

where $\boldsymbol{S}$ is the solution to ARE and the matrix $\boldsymbol{K}$ is given by

$$\boldsymbol{K = R^{-1}R^T S} \quad (11)$$

C. Frequency analysis using singular values

For multi-input/multi-output (MIMO) systems, the individual single-input/single-output (SISO) systems Bode Plot does not provide clear information that allows guaranteed stability or robustness. Therefore, the use of the MIMO Bode Plot of singular values (SV) is a useful tool to design controllers that guarantee stabilize the system at the operating point.

Any matrix $\boldsymbol{M}$ may be written by its singular values decomposition (SVD), as mentioned in [8]. The expression of $\boldsymbol{M}$ from SVD is given as

$$\boldsymbol{M = Y\Lambda V^*} \quad (12)$$

where $\boldsymbol{\Lambda} = diag\{\sigma_1, \sigma_2, \dots, \sigma_i\}$ with $i = rank\{\boldsymbol{M}\}$, both $\boldsymbol{Y}$ and $\boldsymbol{V^*}$ are square unit matrices, and σ_i denotes SV de $\boldsymbol{M}$ which are the square root of the eigenvalues of $\boldsymbol{M^T M}$.

The considerations for Robust State Feedback Controller Design from SV ($\overline{\sigma}$ y $\underline{\sigma}$, maximum and minimum) of the loop gain $\boldsymbol{L_g}$, are the following

1) $\overline{\sigma}(\boldsymbol{L_g})$ should be small at high frequency since disturbances generally predominate in this range and thus guarantee robustness against perturbations.
2) $\underline{\sigma}(\boldsymbol{L_g})$ should be large at low frequency for robust performance against noise signals, for instance, switching noise.
3) The magnitude $\overline{\sigma}$ y $\underline{\sigma}$, for a range of frequencies should have nearby values with the objective that the transient response of all states of the system is similar.
4) The slope of SV around zero crossings in the MIMO Bode plot should be less than 40 dB/dec to guarantee a margin of stability robustness.

For more details about singular values and loop gains, see [8], and [17].

III. LQI CONTROLLER ALGORITHM

The design algorithm of a Linear Quadratic Integral (LQI) controller for the three-phase converter connected to a load, proposed in this work is as follows:

1. Express the system in state space as (1) and discretize the model to bring it into the form as (4). The discretization method is independent in each case.
2. Analytically obtain the open-loop gain $\boldsymbol{L_g}$ of the feedback system, opening the loop at the input signal u.
3. Set the weights of the matrices $\boldsymbol{Q}$ and $\boldsymbol{R}$ to get the feedback gains $\boldsymbol{K}$ from (10) and (11).
4. Select the appropriate frequency range where the controller has the desired behavior.
5. Graph the set of closed-circuit poles of the system for each case obtained in step 4 and carry out their respective step test.
6. Graph the MIMO Bode Plot of $\boldsymbol{L_g}$ and verify the considerations mentioned in section II.C.
7. Select the profit matrix $\boldsymbol{K}$ that satisfies all the design criteria and simulate the system from the structure shown in fig.1, otherwise, return to step 3.

Table I consolidates the values of the components shown in fig.1, among others.

TABLE I. SYSTEM PARAMETERS.

Component	Value	Units
V_{dc}	350	V
R_1	0.01	Ω
L_1	1.8	mH
C_1	8.8	μF
R_2	0.01	Ω
L_2	1.8	mH
R	10	Ω
T_s	100	μs

A. Step 1: State Space Model

To start with the optimal regulator design, matrices $\boldsymbol{A}$, $\boldsymbol{B}$ and $\boldsymbol{C}$ are used from (3), which are subsequently discretized by the ZOH method as described in section II.B. Finally, the state space is increased with the computational delay to be expressed as (8). The sample time is $T_s = 100$ μs (see Table I). The other consolidated values in Table I are used to the numerical solution of the system and simulation of the structure shown in fig. 1.

B. Step 2: Recovery of Robust Loop Gain at the Input

Fig. 2 shows the block diagram proposed to obtain the loop gain $\boldsymbol{L_g}$. Blocks $\boldsymbol{\Phi}$ and $\boldsymbol{\Psi}$ represent the system of (8) and the integrator system in the dq frame, respectively, and both expressed as

$$\boldsymbol{\Phi} = (z\boldsymbol{I} - \boldsymbol{G_d}) \cdot \boldsymbol{H_d}$$
$$\boldsymbol{\Psi} = (z\boldsymbol{I} - \boldsymbol{G_i}) \cdot T_s \cdot \boldsymbol{H_i} \quad (13)$$

with

$$\boldsymbol{G_i} = \begin{bmatrix} \boldsymbol{1} & \boldsymbol{0} \\ \boldsymbol{0} & \boldsymbol{1} \end{bmatrix} \qquad \boldsymbol{H_i} = \begin{bmatrix} \boldsymbol{1} & \boldsymbol{0} \\ \boldsymbol{0} & \boldsymbol{1} \end{bmatrix} \quad (14)$$

After opening the feedback control loop at input $\boldsymbol{u}$ and performing an algebraic matrix operations, the open-loop gain $\boldsymbol{L_g}$, without taken into account the reference signal ($\boldsymbol{V_{ref}} = \boldsymbol{0}$), results as

$$\boldsymbol{L_g} = -(\boldsymbol{K_s\Phi} - \boldsymbol{K_i\Psi C_d\Phi}) \quad (15)$$

$\boldsymbol{K_s}$ and $\boldsymbol{K_i}$ gain matrices for the system considering the delay and the error integrator system, in the framework dq.

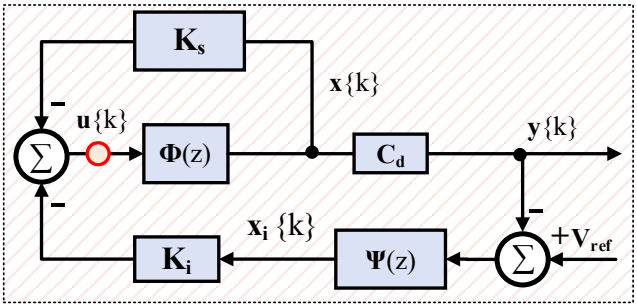

Fig. 2. Block diagram of the feedback system.

C. Step 3: Weighting matrices Q and R

In this step, it is crucial to know the possible weights of $\boldsymbol{Q}$ and $\boldsymbol{R}$ to avoid multiple iterations and then find the feedback gain K_{LQI} until achieving the desired behavior. By heuristics, the most relevant state is the voltage capacitor for island mode since it is desired that the VSC maintains the sine waveform (amplitude and frequency) and achieve to provide it to the load, regardless of a disturbance. However, for the LQI case, the state of the voltage error becomes the most critical state because the objective is to eliminate the output error in steady-state.

From the above, five weight values were selected for this new state variable, and the value of the matrix $\boldsymbol{R}$ was fixed to the identity matrix. Table II summary the costs of these $\boldsymbol{Q}$ matrices. It can be seen that the contribution of the state variable of the voltage error gradually increases with a different rate to the other states. The results of these variations are shown below.

TABLE II. Q MATRIX VARIATIONS.

Q matrix	Value
1	$diag\{1,1,10,100,1000\}$
2	$diag\{1,1,10,100,10000\}$
3	$diag\{1,1,1,10,10000\}$
4	$diag\{1,1,1,1,10000\}$
5	$diag\{1,1,1,1,100000\}$

D. Step 4: Frequency range

The frequency limits allow defining a frequency bandwidth where the controller satisfies the desired performance and robustness of the system based on the criteria mentioned above. In this case, the desired frequency range is defined around 377 rad/sec, the operating frequency of the system.

E. Step 5: Close loop poles and Step Response

The pole movement of the closed-loop system, together with the state of the voltage error for different $\boldsymbol{Q}$ matrices is shown in fig. 3. As seen in Cluster 1, these poles are heading towards the origin but are still far away and are therefore neglected from the point of view of the transient response since they quickly fall to zero, which means that the contribution of these roots is minimal, as indicated in [18]. Observing cluster 2, the movement of the poles on the real axis does not show significant changes since their movement is minimal, and they remain in that neighborhood, but they remain fast poles and are therefore neglected. In cluster 3, as the ratio of the error state increases regarding other states in matrix $\boldsymbol{Q}$ (see Table II), the calculated gain of ARE moves the poles further towards the origin, enough to dominate the response over time and without reaching marginal stability (see zoom in cluster 3). This value begins to increase as the dominant poles move slightly away from the origin, which indicates less overshooting and fewer oscillations in the step response.

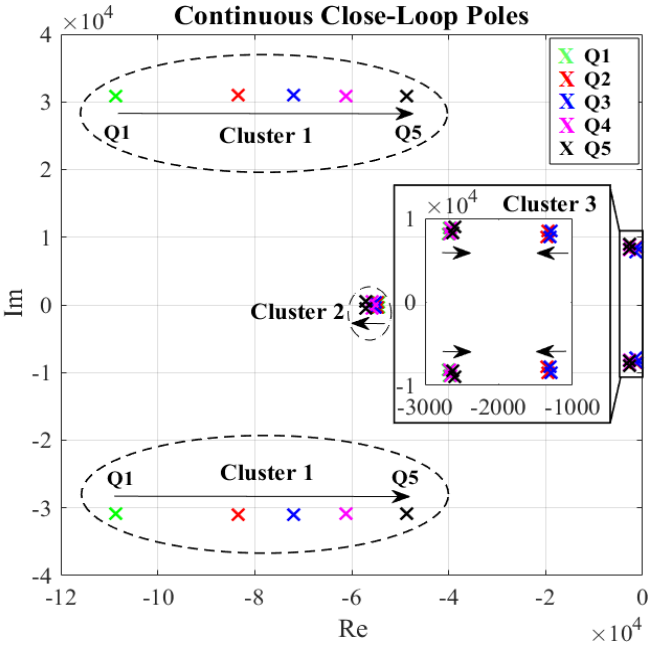

Fig. 3. Close loop poles movement.

The step responses are shown in fig. 4 correspond to the closed-loop system with the five feedback gain matrices. As can be seen, all the paths on the dq-axis, except the response using $\boldsymbol{Q_3}$, behave similarly concerning performance parameters such as overshoot and transient time. Moreover, the response obtained with the matrix $\boldsymbol{Q_5}$ has a shorter establishment time than the others. Therefore, the step response is influential in the selection of the matrix $\boldsymbol{K_{LQI}}$, but it is not precise enough to meet all the design criteria. For this reason, the singular value diagram is generated. It is important to mention that the initial behavior of the step is due to the non-minimum phase zero generated by the computational time delay.

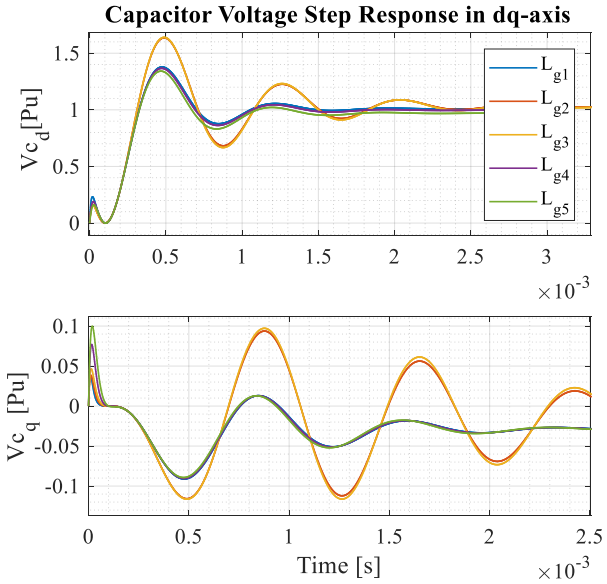

Fig. 4. Capacitor Voltage step responses.

F. *Step 6: Singular values plot*

Fig. 5 shows the diagram of SV of the loop gain $\boldsymbol{L_g}$ obtained in (15). Regarding the considerations raised in section II.D, $\overline{\sigma}$ are below 0 dB in magnitude at high frequencies for all loop gains while $\underline{\sigma}$ of $\boldsymbol{L_{g3}}$, $\boldsymbol{L_{g4}}$ and $\boldsymbol{L_{g5}}$ have a magnitude above 20 dB for low frequency. The paths of these same loop gains show that $\overline{\sigma}$ and $\underline{\sigma}$ have close magnitudes during the frequency sweep. The value of the slope in dB for these three cases of $\boldsymbol{L_g}$ is around 20 dB.

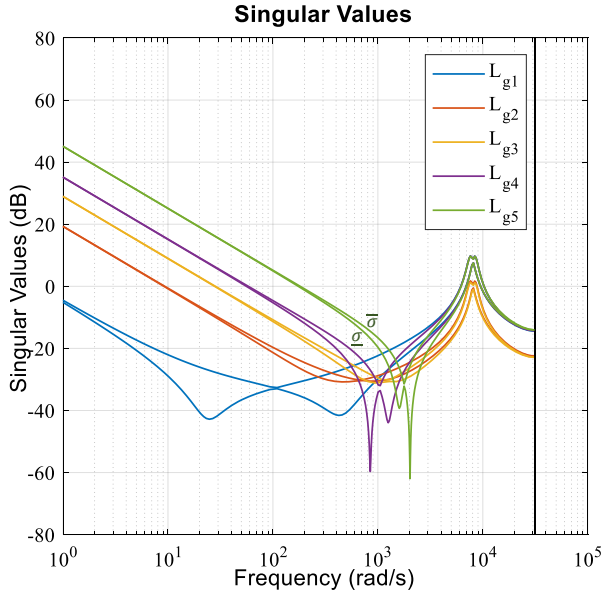

Fig. 5. MIMO Bode Plot of Lg Variations

G. *Step 7: Matrix K selection*

The selected feedback gain matrix $\boldsymbol{K}$ is the one that uses the matrix $\boldsymbol{Q_5}$ according to Table II, since it contains a more significant proportion in the error state, and its contribution improves overshoot and establishment time. The last 4 cases in the SV diagram meet the design criteria, although the magnitude of $\underline{\sigma}$ in $\boldsymbol{L_{g5}}$ achieves a higher gain in low frequency, and for this reason, it improves noise rejection as well as increasing its bandwidth. It is important to remember that the origin in this graph corresponds to the operating angular frequency ω_n due to the transformation in dq.

IV. SIMULATION RESULTS

In order to validate the controller, the structure shown in fig. 1 was simulated using MATLAB® and Simulink® environment. The switching frequency of the PWM is set to 10 kHz, and all the variables are initialized. Simulink runs the entire control system, and the results are exported to MATLAB® for processing. Fig. 6 shows the signal of the dq-frame voltage error in the capacitor. The first transient corresponds to the initial response of the system with initial conditions at zero. In 50 ms, the load step event is generated, reducing its resistance to 50% to verify the expected behavior The overshoot is less than 25%, and the settling time is around 5 ms (see zoom view), which indicates a quick response from the controller against this load change.

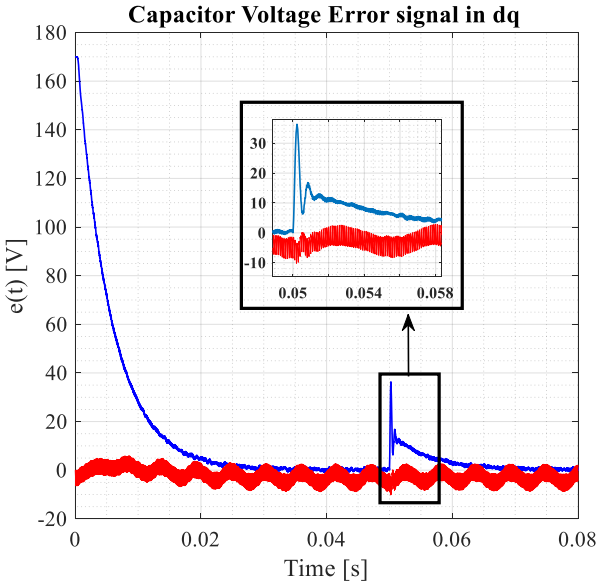

Fig. 6. Capacitor voltage error in dq-axis.

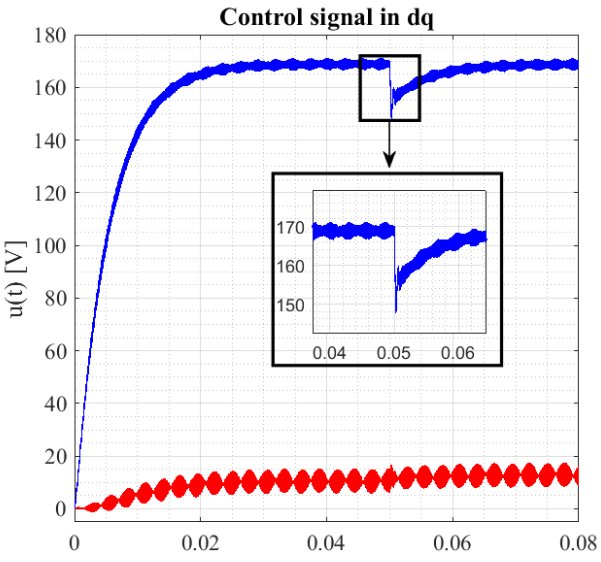

Fig. 7. Controller signal in the dq-axis.

Signal control behavior is shown in fig. 7. There can be appreciated that reference tracking is correct since the

dq signal reaches 170 V and without changes due to the load step. In this event, the modulating signal decrease to 150 V but responds quickly with a set time less than 5 ms, in the same way as the error signal.

Fig. 8 shows the voltage across the capacitor, which has a slight disturbance in all three lines due to the charging step but quickly recovers and stabilizes. Initial behavior is due to initial system conditions.

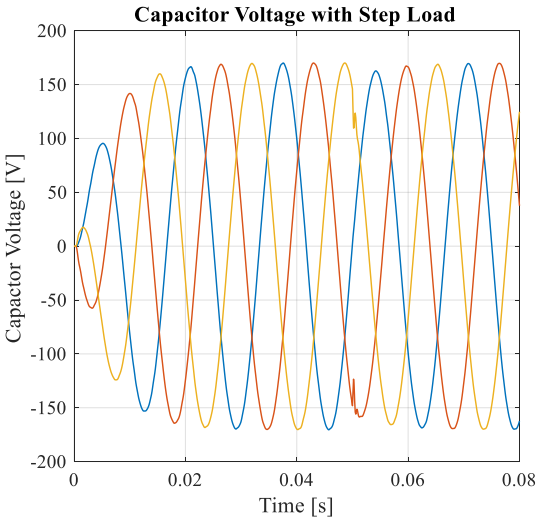

Fig. 8. Capacitor Voltage in the abc-axis.

In fig. 9 the current in the output inductor increases from 1.71A pick to 5.07A pick after the generated event.

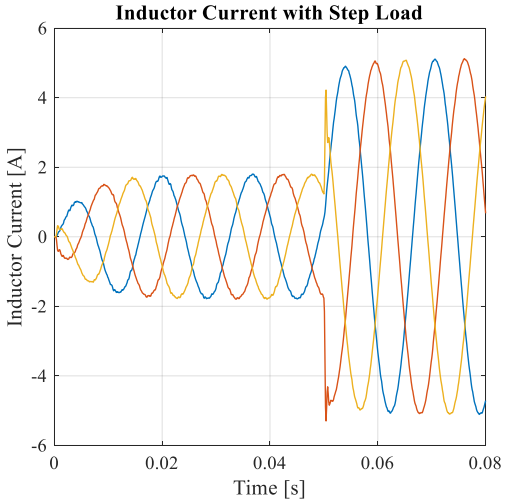

Fig. 9. Current inductor in abc-axis.

CONCLUSION

An algorithm of seven steps to MIMO LQI controllers in VSC was presented. The results show a correct behavior in the transient response (less than 5 ms), slight recovery of the capacitor voltage due to the fast action of the proposed controller against changes in resistive load in an isolated system. In addition, the SV frequency analysis of the feedback system, using MIMO Bode Plot, allows to obtain a better vision of the stability robustness of the control system which the interaction between all the inputs and outputs of the system are taken into account.

REFERENCES

[1] J. M. Guerrero, J. C. Vasquez, J. Matas, L. G. De Vicuña, and M. Castilla, "Hierarchical control of droop-controlled AC and DC microgrids - A general approach toward standardization," IEEE Trans. Ind. Electron., vol. 58, no. 1, pp. 158–172, 2011, doi: 10.1109/TIE.2010.2066534.

[2] H. Athari, M. Niroomand, and M. Ataei, "Review and Classification of Control Systems in Grid-tied Inverters," Renew. Sustain. Energy Rev., vol. 72, no. February, pp. 1167–1176, 2017, doi: 10.1016/j.rser.2016.10.030.

[3] M. Hao and X. Zhen, "A control strategy for voltage source inverter adapted to multi - Mode operation in microgrid," Chinese Control Conf. CCC, pp. 9163–9168, 2017, doi: 10.23919/ChiCC.2017.8028816.

[4] A. Tuladhar, H. Jin, T. Unger, and K. Mauch, "Parallel operation of single phase inverter modules with no control interconnections," in Proceedings of APEC 97 - Applied Power Electronics Conference, 1997, vol. 1, pp. 94–100, doi: 10.1109/APEC.1997.581439.

[5] E. A. A. Coelho, P. C. Cortizo, and P. F. D. Garcia, "Small signal stability for single phase inverter connected to stiff AC system," Conf. Rec. 1999 IEEE Ind. Appl. Conf. Thirty-Forth IAS Annu. Meet. (Cat. No.99CH36370), vol. 4, pp. 2180–2187, 1999, doi: 10.1109/IAS.1999.798756.

[6] N. Pogaku, M. Prodanović, and T. C. Green, "Modeling, analysis and testing of autonomous operation of an inverter-based microgrid," IEEE Trans. Power Electron., vol. 22, no. 2, pp. 613–625, 2007, doi: 10.1109/TPEL.2006.890003.

[7] W. Xiao, P. Kanjiya, J. L. Kirtley, N. H. Kan'an, H. H. Zeineldin, and V. Khadkikar, "A modified control topology to improve stability margins in micro-grids with droop controlled IBDG," in 3rd Renewable Power Generation Conference (RPG 2014), 2014, pp. 5.2.2-5.2.2, doi: 10.1049/cp.2014.0862.

[8] F. L. Lewis, D. L. Vrabie, and V. L. Syrmos, Optimal Control. Hoboken, NJ, USA: John Wiley & Sons, Inc., 2012.

[9] F. Huerta, D. Pizarro, S. Cóbreces, F. J. Rodríguez, C. Girón, and A. Rodríguez, "LQG servo controller for the current control of LCL grid-connected Voltage-Source Converters," IEEE Trans. Ind. Electron., vol. 59, no. 11, pp. 4272–4284, 2012, doi: 10.1109/TIE.2011.2179273.

[10] M. N. Marwali and A. Keyhani, "Control of distributed generation systems - Part I: Voltages and currents control," IEEE Trans. Power Electron., vol. 19, no. 6, pp. 1541–1550, 2004, doi: 10.1109/TPEL.2004.836685.

[11] J. F. Patarroyo-Montenegro, M. Castellà, F. Andrade, K. Kampouropoulos, L. Romeral, and J. Vasquez-Plaza, "An Optimal Tracking Power Sharing Controller for Inverter-Based Generators in Grid-connected Mode," in IECON Proceedings (Industrial Electronics Conference), 2019.

[12] S. Eren, A. Bakhshai, and P. Jain, "Control of three-phase voltage source inverter for renewable energy applications," 2011 IEEE 33rd Int. Telecommun. Energy Conf., pp. 1–4, 2011, doi: 10.1109/INTLEC.2011.6099761.

[13] A. Hasanzadeh, C. S. Edrington, B. Maghsoudlou, and H. Mokhtari, "Optimal LQR-based multi-loop linear control strategy for UPS inverter applications using resonant controller," Proc. IEEE Conf. Decis. Control, pp. 3080–3085, 2011, doi: 10.1109/CDC.2011.6161192.

[14] D. A. L. Robert L. Williams II, Linear State-Space Control Systems, 1st ed. Wiley, 2007.

[15] R. Teodorescu, M. Liserre, and P. Rodriguez, Grid Converters for Phovoltaic and Wind Power Systems. John Wiley & Sons, Inc., 2011.

[16] J. F. Patarroyo-Montenegro, J. E. Salazar-Duque, and F. Andrade, "LQR Controller with Optimal Reference Tracking for Inverter-Based Generators on Islanded-Mode Microgrids," in 2018 IEEE ANDESCON, 2018, pp. 1–5, doi: 10.1109/ANDESCON.2018.8564638.

[17] J. M. MacIejowski, Multivariable feedback design. Addison-Wesley, 1989.

[18] K. Benjamin, Sistemas de Control Automatico, 7th ed. Prentice Hall, 1997.